J. Fluid Mech. (2011), *vol.* 688, *pp.* 551–568.
doi:10.1017/jfm.2011.403

A numerical study of an inline oscillating cylinder in a free stream

Justin S. Leontini[1]†, David Lo Jacono[1,2,3] and Mark C. Thompson[1]

[1] Fluids Laboratory for Aeronautical and Industrial Research (FLAIR), Department of Mechanical and Aerospace Engineering, Monash University, Melbourne, VIC 3800, Australia

[2] Université de Toulouse; INPT, UPS; IMFT (Institut de Mécanique des Fluides de Toulouse), Allée Camille Soula, F-31400 Toulouse, France

[3] CNRS; IMFT; F-31400 Toulouse, France

(Received 16 March 2011; revised 25 August 2011; accepted 17 September 2011; first published online 3 November 2011)

Simulations of a cylinder undergoing externally controlled sinusoidal oscillations in the free stream direction have been performed. The frequency of oscillation was kept equal to the vortex shedding frequency from a fixed cylinder, while the amplitude of oscillation was varied, and the response of the flow measured. With varying amplitude, a rich series of dynamic responses was recorded. With increasing amplitude, these states included wakes similar to the Kármán vortex street, quasiperiodic oscillations interleaved with regions of synchronized periodicity (periodic on multiple oscillation cycles), a period-doubled state and chaotic oscillations. It is hypothesized that, for low to moderate amplitudes, the wake dynamics are controlled by vortex shedding at a global frequency, modified by the oscillation. This vortex shedding is frequency modulated by the driven oscillation and amplitude modulated by vortex interaction. Data are presented to support this hypothesis.

Key words: pattern formation, vortex shedding, vortex streets

1. Introduction

This paper studies the controlled oscillation of a cylinder in a free stream. The problem of an oscillating cylinder generates considerable research interest, from both a fundamental fluid-structure interaction point of view and an applications-based point of view. With regards to the latter, a driving factor has been to understand the physics inherent to the problem of vortex-induced vibration (VIV). This focus has led to many studies of cylinders oscillating transverse to the free stream, as this is the primary direction of oscillation during VIV.

However, an inline component of motion has been shown to play a major role in VIV, as the structure responds to the fluctuating drag force. Jauvtis & Williamson (2005) showed a unique '2T' mode of vortex shedding, consisting of two triplets of vortices per oscillation cycle, which occurred when inline oscillation was allowed during VIV experiments, with repercussions for the fluid loading of structures. Recently, Horowitz & Williamson (2010), in experiments on rising and falling

† Email address for correspondence: justin.leontini@monash.edu

cylinders (essentially VIV with no restoring spring force or mechanical damping), showed that, for such a body to oscillate at all, an equivalent elastically mounted system requires the natural frequency in the inline direction to be twice the natural frequency in the transverse direction.

This fact appears naturally, as the drag force typically fluctuates at twice the frequency of the lift. Because of this, many studies of driven inline oscillations have concentrated on forcing at frequencies at, or close to, twice the Strouhal frequency, f_{St} (see e.g. Tanida, Okajima & Watanabe 1973; Barbi *et al.* 1986; Karniadakis & Triantafyllou 1989; Konstantinidis, Balabani & Yianneskis 2005; Konstantinidis & Balabani 2007), where the Strouhal frequency is the frequency of the vortex shedding from a stationary cylinder. Forcing at these frequencies leads to synchronization of the vortex shedding to the oscillation frequency; however, as the frequency is moved away from $2f_{St}$, the amplitude required to maintain this synchronization increases (Griffin & Hall 1991).

Aside from the direct practical application to VIV, the problem of a controlled, sinusoidal, inline oscillation can present a unique viewpoint in terms of wake control strategies. The impact of cylinder motion on the wake has been extensively studied, using a range of motions. A plethora of studies on sinusoidal transverse oscillations exist – see e.g. Bishop & Hassan (1964), Koopman (1967), Staubli (1983), Carberry, Sheridan & Rockwell (2005) and Leontini *et al.* (2006) and Morse & Williamson (2009), and the reviews of Williamson & Govardhan (2004) and Sarpkaya (2004) and references therein. The studies of Thiria, Goujon-Durand & Wesfreid (2006) and Thiria & Wesfreid (2007) investigated the behaviour of the two-dimensional wake of a cylinder performing rotational oscillations. These studies have shown that, if the oscillation frequency is close to the Strouhal frequency f_{St}, the wake remains synchronized to the oscillation frequency.

It should be noted that the symmetry of the forcing introduced by both the transverse and rotational oscillations is the same as that of the unperturbed wake (i.e. the spatio-temporal symmetry of reflection about the wake centreline plus evolution forwards by half a period). Nazarinia *et al.* (2009) studied the wake of a cylinder undergoing combined rotational and transverse oscillations. This study found that the synchronization was a function of the phase between the transverse and rotational oscillations, and therefore a function of the symmetry of the forcing.

Inline oscillations do not share this symmetry, a fact cited by Ongoren & Rockwell (1988) as being of importance in the synchronization process. Feng & Wang (2010) used a synthetic pulsating jet at the rear of the cylinder, thereby providing a forcing of the same symmetry as inline driving. The results of this study showed that this type of forcing could have a significant impact on the vortex formation process, and therefore the synchronization process.

Focusing on studies of inline driving of a cylinder, Griffin & Ramberg (1976) performed experiments investigating the range of frequencies of oscillation for which the flow synchronized to the driving frequency. They found a lock-in region at frequencies centred around twice the Strouhal frequency. Interestingly, they found two modes of vortex shedding in this synchronization regime: one where a pair of opposite-sign vortices was shed per period (regime I in the notation of Griffin & Ramberg 1976); and one where a single vortex was shed per period of oscillation, and another vortex of opposite sign was shed in the following period (regime II in the notation of Griffin & Ramberg 1976). These two modes could be thought of as a primary and subharmonic synchronization, respectively. Both modes appeared to retain the staggered arrangement of vortices in a typical bluff-body wake.

Ongoren & Rockwell (1988) performed an extensive set of experiments for $A^* = A/D = 0.13$, for frequency ratios $0.5 \leqslant f_d/f_{St} \leqslant 4.0$, where A is the amplitude of oscillation, D is the cylinder diameter, f_d is the frequency of driven oscillation and f_{St} is the Strouhal frequency. In these experiments, multiple synchronization regions were found. The first was again where $f_d/f_{St} \simeq 2$; however, synchronization also occurred for $f_d/f_{St} > 3$, but to a symmetric mode of vortex shedding, which consisted of two vortices per oscillation period of opposite sign, symmetrically opposed about the wake centreline. They observed mode competition between these symmetric and anti-symmetric modes in between these synchronization regions. This mode competition has also been observed by Konstantinidis & Balabani (2007).

Cetiner & Rockwell (2001) performed similar experiments, taking detailed force measurements for a series of amplitudes over a frequency range $0.37 \leqslant f_d/f_{St} \leqslant 3.0$. At higher amplitudes of oscillation (approaching $A^* = 1$ in some cases), a further synchronization region was observed in the vicinity of $f_d/f_{St} = 1$. Similar to the result of Griffin & Ramberg (1976) around $f_d/f_{St} = 2$, their force traces indicate that this synchronization could occur through a primary or subharmonic synchronization, but appear to show subharmonic synchronization for $A^* > 0.3$. Synchronization to a subharmonic mode at high amplitudes when $f_d/f_{St} = 1$ was also reported in the experiments of Barbi *et al.* (1986) for Reynolds numbers as high as 40 000.

Al-Mdallal, Lawrence & Kocabiyik (2007) reported a quasiperiodic state for oscillations at $f_d/f_{St} = 1$ when $A^* = 0.1$. Experiments from Kim & Williams (2006) using very small amplitudes of oscillation and a frequency ratio $f_d/f_{St} = 0.77$ reported a decrease in the primary frequency of vortex shedding from the cylinder. The power spectrum of the lift force generated showed a series of frequencies present, all of which were related to the primary vortex shedding frequency f_s or the driving frequency f_d. The series they found contained frequencies f_s, and then $f_s \pm nf_d$, where n is a positive integer. Konstantinidis & Bouris (2009) did computations of a pulsated flow past a cylinder (a dynamically equivalent problem to the inline driven cylinder) where the waveform of the pulsation was varied from the classical sinusoidal oscillation by adding other frequency components. Changing the extra frequency components was shown to have a major impact on the vortex shedding process and the wake modes present.

Perdikaris, Kaitsis & Triantafyllou (2009) presented data from two-dimensional simulations for a Reynolds number of 400 for a range of amplitudes for a fixed frequency, where $f_d/f_{St} = 1$. For low amplitudes, they observed an apparent primary synchronization to the classic anti-symmetric mode. At high amplitudes, they observed a subharmonic synchronized wake, again with an anti-symmetric staggering of vortices. At intermediate amplitudes, they reported observing either quasiperiodicity or chaos in the wake. The chaotic state was attributed to mode competition.

These results showing a range of possible states depending on A^*, particularly at $f_d/f_{St} = 1$, show that the synchronization phenomenon, and the state selection process, contain many transitions. These results suggest that the qualitative picture of a simple synchronization region focused around $f_d/f_{St} = 1$ that has only a single critical amplitude for synchronization, as presented by Karniadakis & Triantafyllou (1989) and in the review paper of Griffin & Hall (1991), may not be fully representative.

The current paper seeks to further investigate these synchronization and state selection phenomena. Keeping the driving frequency f_d constant so that $f_d/f_{St} = 1$, a series of simulations have been conducted at fine increments of amplitude. It is shown that, at intermediate amplitudes, the flow is not chaotic, but is, in general, quasiperiodic, with two incommensurate frequencies driving the dynamics. Interleaved

in this quasiperiodic region are bands of P_N periodic response, where P_N denotes a response that has a period of N cycles of oscillation.

These bands of resonance to P_N states are shown to occur when the primary frequency of vortex shedding makes an integer ratio with the driving frequency. As this primary frequency of vortex shedding is shown to be a function of the amplitude of oscillation, this is interpreted in terms of a dispersion relation. The frequency content of the response is explained by considering the cylinder as a wave generator, coupled with the frequency modulation of these waves by the oscillatory driving, and the amplitude modulation due to vortex interaction in the wake.

2. System definition and methodology

The system studied was that of a circular cylinder immersed in a free stream, undergoing sinusoidal oscillations parallel to the flow direction. These oscillations were of the form

$$\frac{x_{cyl}}{D} = A^* \sin(2\pi f_d \tau), \tag{2.1}$$

where x_{cyl} is the cylinder's relative displacement from its neutral position, and $\tau = tU/D$ is the non-dimensional time, where t is time, and U is the free stream velocity. Note that the frequency of oscillation was set to the Strouhal frequency of the fixed cylinder, f_{St}, so that $f_d/f_{St} = 1$. The Reynolds number, $Re = UD/\nu$, where ν is the kinematic viscosity, was set to $Re = 175$, below, but close to, the critical value of $Re \simeq 190$ for the transition to a three-dimensional flow in the fixed cylinder case (Williamson 1988). Using a value so close to the threshold may mean that the flow is actually three-dimensional (it cannot be known *a priori* if the oscillation will be destabilizing on the wake). Results from a simulation at $Re = 100$ are provided in § 3.5 that show a flow with the same characteristics as the flows at $Re = 175$. This provides a high level of confidence that the results gained should generalize to other values of Re where the flow is two-dimensional.

Therefore, two-dimensional direct numerical simulations were performed, solving the incompressible Navier–Stokes equations using a highly accurate spectral-element method (Thompson, Hourigan & Sheridan 1996). Seventh-order tensor-product Lagrange polynomials, associated with Gauss–Legendre–Lobatto quadrature points, were used as shape functions. A three-way time splitting scheme was used for time integration, which formed a Poisson equation that was solved for the pressure field (Karniadakis, Israeli & Orszag 1991). A third-order Adams–Bashforth method was used to solve the resulting equation for the advection term, and a second-order Crank–Nicholson method was employed for the diffusion term.

To account for the cylinder motion, the Navier–Stokes equations were solved in the frame of reference attached to the cylinder. As this frame is non-inertial, an extra term for the frame acceleration was added to the equations. This approach requires no mesh deformation, maintaining the speed and accuracy of the method over the entire simulation time. This code has been employed and extensively verified in previous similar studies, including three-dimensional cylinder simulations (Thompson *et al.* 1996), transversely oscillating cylinder studies (Leontini *et al.* 2006; Leontini, Thompson & Hourigan 2007) and rotationally oscillating cylinder studies (Lo Jacono *et al.* 2010).

Dirichlet boundary conditions were applied at the cylinder surface ($u_x = u_y = 0$), and at the inlet and side boundaries ($u_x = 1$, $u_y = 0$, or free stream conditions). Here, u_x and u_y are the velocity in the streamwise and cross-stream directions, respectively.

Polynomial order	f_{St} (fixed)	$C_{l_{MAX}}$ (fixed)	$C_{l_{MAX}}$ ($A^* = 0.5$)
5	0.193 33	0.616 26	2.023 67
6	0.193 34	0.615 75	2.022 20
7	0.193 30	0.614 54	2.020 67
8	0.193 32	0.615 19	2.028 41

TABLE 1. Results of a resolution test on a fixed cylinder, and the inline oscillating cylinder, for $A^* = 0.5$. The frequency of shedding varies by less than 0.1 % for shape function polynomial orders 5–8 for the fixed cylinder, and the peak lift coefficient for the converged periodic solution for both the fixed and oscillating cylinder varies by less than 1 %. A polynomial order of 7 has been used for the simulations of the current study.

A zero-normal gradient condition was applied at the domain outlet, as well as fixing the pressure. This outlet was set at least $50D$ downstream of the cylinder.

A resolution test was conducted for the macro-element mesh employed by varying the polynomial order of the shape functions in each element. Simulations of a fixed cylinder at $Re = 175$, and simulations of the inline oscillating cylinder, with $A^* = 0.5$, were run. The Strouhal frequency f_{St} and the maximum lift coefficient of the converged limit cycle oscillations were compared for the fixed cylinder. As the frequency of oscillation was set at f_s for the driven oscillation simulations, only the maximum converged lift coefficient was compared. The numbers obtained are provided in table 1. In both cases, the lift coefficient varied by less than 1 % for polynomial orders from 5 to 8, and f_{St} varied by less than 0.1 % over the same range. This provides a high degree of confidence that the results of the current study, using seventh-order polynomials, are adequately resolved.

3. Results and discussion

3.1. *The identification of response regimes*

Response regimes were identified with the aid of Poincaré maps. These maps were produced by sampling the time history of the lift and drag coefficients on the cylinder at the driving frequency, and plotting the result. Any transient (typically the signal before $\tau = 200$) was discarded so that the Poincaré maps represented only the long-time dynamics.

Examples of the maps produced, for four values of A^*, are presented in figure 1. These examples show a quasiperiodic response, a P_6 response, synchronization to the subharmonic mode (which could equally be labelled a P_2 mode) and a chaotic response. The quasiperiodic response draws a filled curve in the Poincaré map, the P_N modes produce N distinct points, and the chaotic response essentially fills a bound region with points if a long enough time history is used.

For amplitudes below that at which the onset of the subharmonic mode was found ($A^* = 0.38$), only quasiperiodic and P_N periodic responses were found. This finding is in conflict with the conclusion that the flow appears chaotic drawn by Perdikaris *et al.* (2009), who reported a small band of chaos for amplitudes $0.18 \leqslant A^* \leqslant 0.23$. However, the Reynolds number in their simulations was also $Re = 400$, as opposed to the value of $Re = 175$ used for the data of figure 1. It is therefore possible that the emergence of chaos at amplitudes close to $A^* = 0.2$ is a function of Re. Perdikaris *et al.* (2009) did report that they also observed chaos at these amplitudes for $Re < 190$; however, those

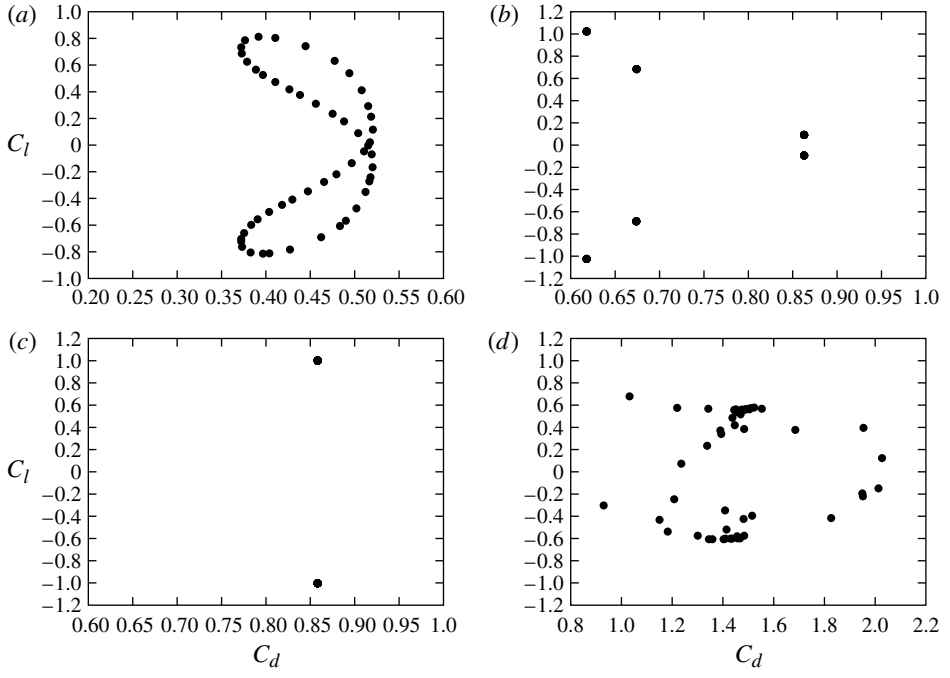

FIGURE 1. Poincaré maps for (*a*) $A^* = 0.17$, (*b*) $A^* = 0.29$, (*c*) $A^* = 0.40$ and (*d*) $A^* = 0.65$. These show the signatures of quasiperiodicity, P_6 response, subharmonic synchronization (or P_2 response) and chaotic response, respectively. These plots are of the lift coefficient C_l versus drag coefficient C_d, both sampled at the driving frequency.

results were not published due to space restrictions, so it is not clear exactly which values of *Re* were tested. Further work is required to fully understand this discrepancy.

To summarize the results of these Poincaré maps, the sampled values of C_l in each have been used to produce a type of bifurcation diagram, as shown in figure 2.

The diagrams presented in figure 2 clearly show the interleaving of regions of quasiperiodicity with P_N periodicity for $A^* < 0.38$. In the diagram, quasiperiodicity is indicated by a filled column of points for a given value of A^*, whereas P_N periodicity is indicated by a column containing exactly N points. (As an aside, a chaotic response would also appear as a full column, and an inspection of the Poincaré map for each case is required to distinguish between them.)

Inspection of figure 2(*b*) shows a clear progression in the appearance of the P_N regimes. With increasing A^*, N is reduced by one at each subsequent P_N regime. For example, a P_8 response is indicated at $A^* = 0.24$, then a P_7 response at $A^* = 0.26$, then a P_6 response at $0.28 \leqslant A^* \leqslant 0.29$, etc. This continues until the subharmonic synchronization (P_2) at $A^* = 0.38$. Only a P_3 response is missing from the progression. This response may well be possible, as no effort has been made to establish the full range of extent of each of these modes, or to study the nature of the bifurcation from one to the other. It is possible that, for some values of A^*, the flow is bistable, and the response selected by the flow is a function of the initial conditions. All of the simulations for the current study were started from rest.

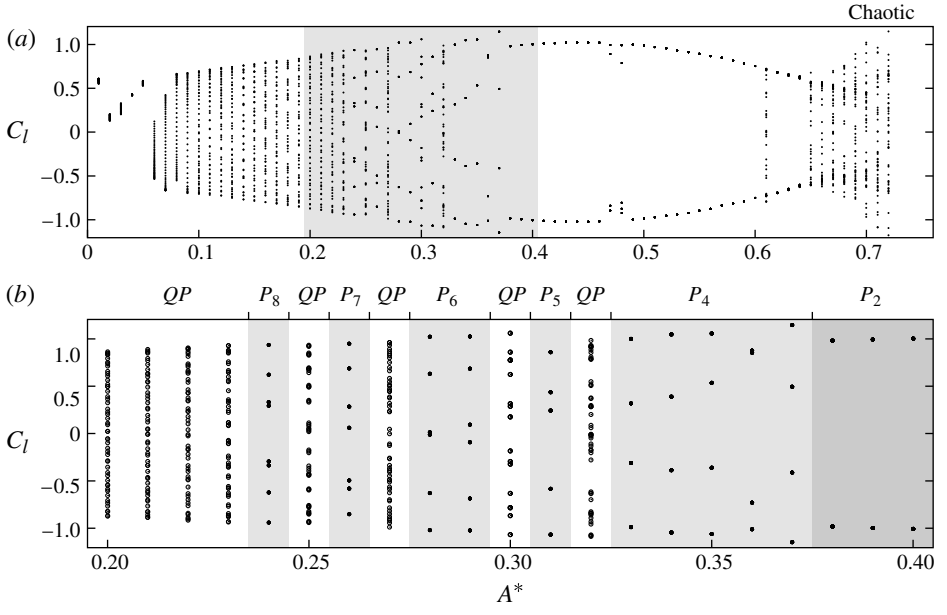

FIGURE 2. (*a*) Values of the lift coefficient C_l sampled at the driving frequency versus the driving amplitude A^*. A subharmonic synchronization is shown for $A^* \geqslant 0.38$, where only two values of C_l are recorded. Quasiperiodicity is interleaved with regions of P_N periodicity for $A^* < 0.38$. (*b*) Expanded plot of the area denoted by the grey box in panel (*a*). The P_N responses are highlighted with a grey box.

It appears that these P_N responses are a resonance between a new global frequency (the frequency of the vortex shedding) and the driving frequency. Further explanation of this point is given in § 3.6.

For values of $A^* > 0.65$, the picture is not as clear. For these higher amplitudes, the response can be quite complicated, and appears to be truly chaotic (at least for selected values of A^*). Further work is required to fully characterize this region, and to gain an understanding of the wake dynamics.

The vortex shedding modes associated with each of the identified P_N response regimes are presented in figure 3. The images of figure 3 show that the number of vortices is not a simple linear function of N. In these response regimes, the flow is attempting to lock to a subharmonic of the oscillation frequency (see § 3.6), and because of this the vortex formation and shedding process can become quite complicated.

3.2. *Frequency content of the lift and drag signal*

3.2.1. *Fourier analysis of the lift and drag*

Further information regarding this system's response is gained by inspection of the frequencies present. For each value of A^*, the frequency content of the lift and drag signals has been obtained from a fast Fourier transform (FFT). Examples of the spectra produced, along with time series of the lift signal, are presented in figure 4. The cases presented are the same as those used to produce the Poincaré sections of figure 1.

To build a picture of the variation of the frequencies present with increasing A^*, the spectra from each value of A^* have been stacked next to each other. This presents the energy content as a function of frequency and A^*, as shown in figure 5. In this figure,

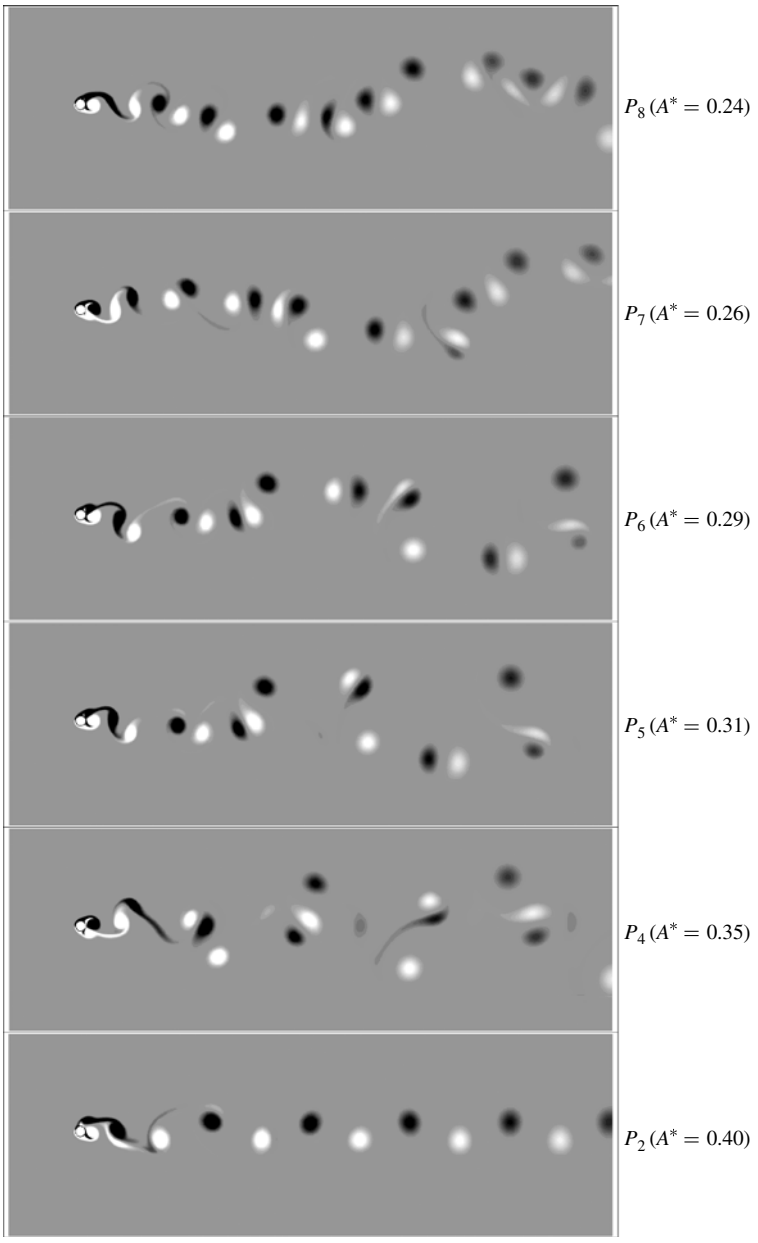

FIGURE 3. Snapshots of vorticity in the wake for all the P_N regimes. With increasing A^*, N decreases. The images show that, while the forces on the cylinder are N periodic, the vortex shedding process and subsequent wake structures are highly complex, and the number of vortices shed per cycle is not simply a linear function of N.

the energy content of each frequency is represented by the greyscale contours in the A^*–f_d/f_{St} plane, for both the lift and the drag force.

3.2.2. *Estimation of the dispersion relation from the data*

If the amplitude of oscillation is considered as a characteristic wavelength, a dispersion relation, relating this wavelength to the global frequency of the resulting

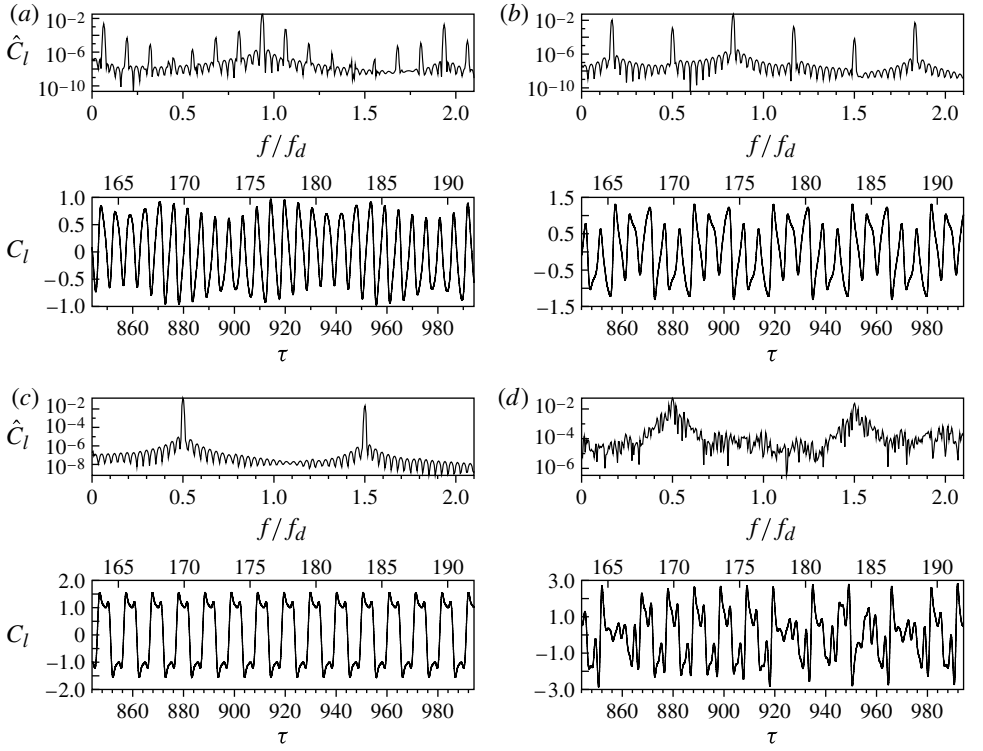

FIGURE 4. Power spectrum and time series of lift for (*a*) $A^* = 0.17$, (*b*) $A^* = 0.29$, (*c*) $A^* = 0.40$ and (*d*) $A^* = 0.65$. These show the signatures of quasiperiodicity, P_6 response, subharmonic synchronization (or P_2 response) and chaotic response, respectively.

vortex shedding, can be obtained from the data. To do this, the primary frequency of response from the lift force (which is equal to the new vortex shedding frequency, f_s) has been extracted for each A^* prior to the synchronization to the subharmonic mode at $A^* = 0.38$. Points where the flow is P_N periodic have been discarded (as the synchronization phenomenon leads to a change in the vortex shedding frequency trend), leaving only the quasiperiodic cases. A power-law curve has then been fitted in a least-squares sense to these points, leading to the relation

$$f_s = f_d(1 - 2.21A^{*2.02}). \tag{3.1}$$

Note that the power is very close to 2. Perdikaris *et al.* (2009) suggested that the variation of this frequency was with A^{*2} for small amplitudes. The data presented here suggest that variation of f_s with A^{*2} may hold up to moderate amplitudes.

Equation (3.1) is plotted as the heavy solid line in figure 6. The figure shows that the curve represents the trend of the data very well, as it closely follows the points extracted from the data.

3.3. *Phase modulation of the vortex shedding by the oscillatory driving*

Inspection of figure 5(*b*), which shows the variation of the frequency content of the lift force with respect to A^*, shows that the frequency response of the flow can be very rich. For $A^* \leqslant 0.38$ (prior to the synchronization to the subharmonic, or P_2 mode), while the majority of the energy is contained in the component at the

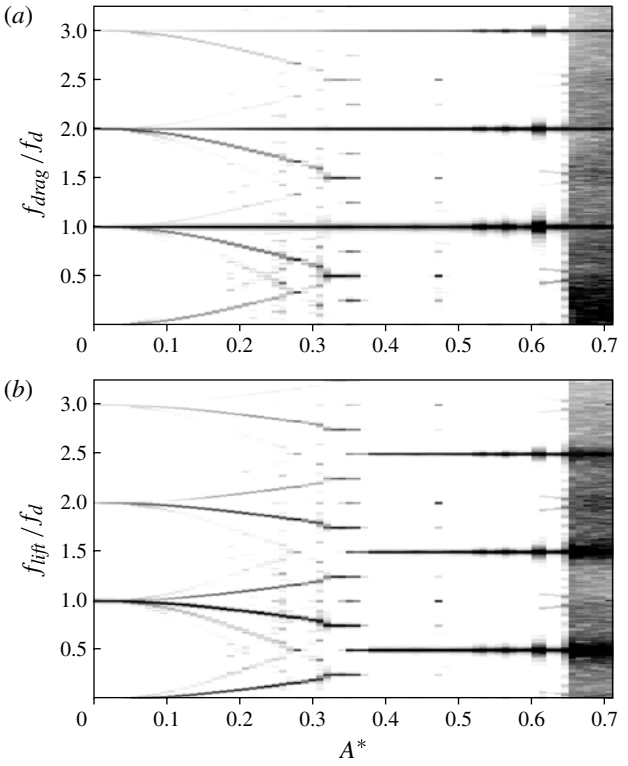

FIGURE 5. Frequency content of (*a*) the drag force and (*b*) the lift force signal as a function of A^*. The energy in each frequency component is represented by the greyscale contours. For the lift force, the strongest frequency component is that at the primary vortex shedding frequency, followed by the sum and difference between the primary vortex shedding frequency and the driving frequency. For the drag force, the strongest frequency component is that at the driving frequency, again followed by the sum and difference between the primary vortex shedding frequency and the driving frequency.

primary shedding frequency f_s, a whole series of frequencies is present. This frequency series appears to vary smoothly with A^* over this range (with apparently only minor consideration of whether the flow is quasiperiodic or P_N periodic).

It is proposed that this frequency series can be explained by considering the oscillating cylinder as a wave generator, sending waves down the wake. In fact, these waves are the vortex shedding. The frequencies present in this series can then be defined and explained by considering the interaction between the driving frequency, f_d, and the frequency of these generated waves, or vortex shedding, f_s.

The first step to this explanation is to identify the frequencies present in the flow response. Figure 6 presents the six strongest frequencies present in the lift force, extracted from the data presented in figure 5. These correspond to the six highest peaks in the spectra for each A^*, such as those presented in figure 4. No filtering or preferential selection has been applied; simply the frequencies at which the six highest peaks occur have been selected. These frequencies are represented by the points in figure 6.

The strongest frequency is always that at the primary vortex shedding frequency, f_s. The variation of this frequency with increasing A^* is well described by the relation

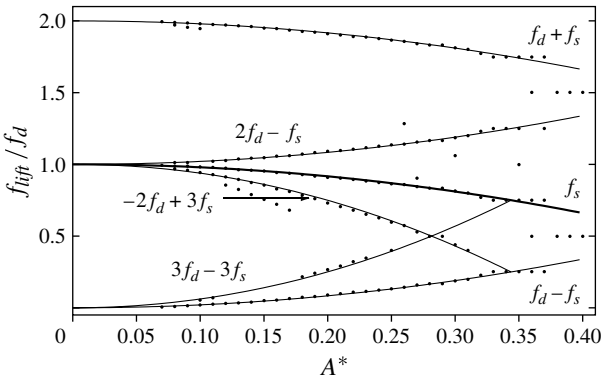

FIGURE 6. The six most energetic frequencies of the lift force data, as a function of A^*. The black points indicate the frequencies extracted from the lift data presented in figure 5. The heavy solid line represents a curve fitted to the primary frequency of response, f_s. The other solid lines are combinations of the curve fitted to f_s with the driving frequency. Note that all frequencies have been normalized by the driving frequency f_d (this has not been included in the labels on the plot so that the labels do not obstruct the data). The data points generally follow the lines very closely.

defined in (3.1). This relation is shown as the heavy solid line in figure 6. All the other lines on the figure have then been generated by combining this relationship, or integer multiples of it, with integer multiples of the driving frequency f_d.

The match between the extracted frequencies and the curves is extremely good, with almost all the extracted points falling on, or near, the curves. This provides a certain level of confidence that the frequency response can be described in terms of frequencies constructed from the sum and difference of integer multiples of the primary shedding frequency, f_s, and the driving frequency, f_d. For clarity, these frequency components have been ranked in terms of strength, and their definitions stated in table 2.

As suggested above, these frequencies can be explained by considering the body as a wave generator. Consider the system in the frame of reference moving with the cylinder. In this frame, waves are primarily generated at the new vortex shedding frequency, f_s. These waves will travel down the wake at some finite speed, inducing a phase, ϕ, between the wave generation at the cylinder and its measurement. Therefore, the general form of a signal measured in the wake will be

$$\psi(x) = \zeta(x)\sin(2\pi f_s \tau + \phi), \tag{3.2}$$

where $\psi(x)$ is the measured quantity, $\zeta(x)$ is the amplitude of the wave, and x is the distance downstream of the cylinder in the moving frame of reference. The phase ϕ is dependent on the distance downstream where the measurement is taken, and the speed at which waves are convected downstream. The wave speed comprises two terms: the first is the convection speed in the frame of reference, c; the second comes from the fact that the frame of reference is accelerating in the direction of wave propagation (i.e. inline with the flow) sinusoidally. Therefore, ϕ is of the form

$$\phi(x) = \frac{x}{c} + 2\pi f_d A^* \sin(2\pi f_d \tau). \tag{3.3}$$

Term	Frequency	Model coefficient	Normalized model coefficient
1	f_s	$\zeta J_0(\alpha)$	1
2	$f_s + f_d$	$\zeta J_1(\alpha)$	$\xi_1 = J_1(\alpha)/J_0(\alpha)$
3	$f_s - f_d$	$\zeta(1+\Gamma)J_1(\alpha)$	$\xi_2 = (1+\Gamma)J_1(\alpha)/J_0(\alpha)$
4	$3f_s - 2f_d$	$\zeta\Gamma J_0(\alpha)$	$\xi_3 = \Gamma$
5	$f_s - 2f_d$	$\zeta(\Gamma/J_0(\alpha) - J_2(\alpha))$	$\xi_4 = (\Gamma - J_2(\alpha)/J_0(\alpha))$
6	$3f_s - 3f_d$	$\zeta\Gamma J_2(\alpha)$	$\xi_5 = \Gamma J_2(\alpha)/J_0(\alpha)$

TABLE 2. Definitions of the six most prominent frequencies in the lift force, listed in order of strength, presented in figure 6. Also presented are the coefficients of the frequency and amplitude modulated model for the lift force for these frequency components presented in (3.10).

This results in an equation for the measured signal at a given point being

$$\psi(x) = \zeta(x)\sin\left(2\pi f_s\tau + \frac{x}{c} + 2\pi f_d A^*\sin(2\pi f_d\tau)\right), \tag{3.4}$$

or one sinusoid at the vortex shedding frequency, f_s, phase-modulated by a second sinusoid at the driving frequency, f_d. If $\psi(x)$ is considered as the force on the body (at $x = 0$), the resulting signal is

$$\psi = \zeta\sin(2\pi f_s\tau + 2\pi f_d A^*\sin(2\pi f_d\tau)). \tag{3.5}$$

This phase-modulated signal can be decomposed (Chowning 1973) as

$$\begin{aligned}\psi = \zeta\{&J_0(\alpha)\sin(2\pi f_s\tau) + J_1(\alpha)[\sin(2\pi(f_s+f_d)\tau) - \sin(2\pi(f_s-f_d)\tau)]\\ &- J_2(\alpha)[\sin(2\pi(f_s+2f_d)\tau) + \sin(2\pi(f_s-2f_d)\tau)]\\ &+ J_3(\alpha)[\sin(2\pi(f_s+3f_d)\tau) - \sin(2\pi(f_s-3f_d)\tau)] + \cdots\},\end{aligned} \tag{3.6}$$

where J_N is the Bessel function of the first kind of order N and $\alpha = 2\pi f_d A^*$.

Essentially, this decomposition indicates that, if the lift force is generated purely by the vortex shedding at the new vortex shedding frequency f_s that is phase (or equivalently, frequency) modulated by the driving frequency f_d, the spectrum should contain the new global frequency f_s, and components at frequencies that are the sum and difference between f_s and integer multiples of the driving frequency f_d. The magnitudes of these components should also scale according to the series of Bessel functions $J_N(\alpha)$.

Inspection of the frequencies presented in table 2 shows that the first three measured frequencies are the same as the frequencies of the first three terms of (3.6). The fifth frequency in table 2 is also present as the fifth term of (3.6). However, (3.6) cannot account for the fourth and sixth frequencies, indicating that this model needs augmenting to more fully describe the wake dynamics.

3.4. *Amplitude modulation in the wake*

The extra frequencies present can be accounted for by adding an amplitude modulation to the frequency-modulated model of (3.6), if it is assumed that this amplitude modulation occurs at a frequency of $2(f_s - f_d)$.

Inspection of the time series of the lift force in figure 4 (focusing on panels (*a*) and (*b*), the examples for which $A^* < 0.4$) clearly shows that the lift force is amplitude modulated. It is proposed that this amplitude modulation is due to the modification of the location and strength of the shed vortices each oscillation cycle, because the

shedding occurs at a different phase of the oscillation cycle. This phase cycles from 0 to 2π with a frequency of $f_s - f_d$. The strongest vortices will be shed when they are formed as the body is moving against the free stream, increasing shear and vorticity production. This stronger vortex will produce a larger force. This means that the vortex formed on the other side of the wake, approximately half an oscillation cycle later, will be formed as the body is moving with the free stream, decreasing its strength. However, this weaker vortex will remain closer to the cylinder for longer (as the body is moving in the same direction as the flow), therefore having a large impact on the force on the body.

If this argument holds, it should be invariant as to which side has the stronger vortex, and which has the weaker, but closer, vortex. Therefore, the modulation it creates should occur at both positive and negative values of the phase between the oscillation and the vortex shedding, and therefore repeat twice as the phase cycles from 0 to 2π, which is what is observed.

Applying this amplitude modulation to the frequency modulation model of (3.6) leads to a model for the lift force of

$$\begin{aligned}\psi = {} & \{1 + \Gamma[\sin(2\pi(f_s - f_d)\tau)]\} + \zeta\{J_0(\alpha)\sin(2\pi f_s\tau) \\ & + J_1(\alpha)[\sin(2\pi(f_s + f_d)\tau) - \sin(2\pi(f_s - f_d)\tau)] \\ & - J_2(\alpha)[\sin(2\pi(f_s + 2f_d)\tau) + \sin(2\pi(f_s - 2f_d)\tau)] + \cdots\},\end{aligned} \tag{3.7}$$

where Γ controls the magnitude of the amplitude modulation. Rewriting the product of sinusoids using the identity

$$\sin(A)\sin(B) = \sin(A + B) + \sin(A - B), \tag{3.8}$$

(3.7) can be written as

$$\begin{aligned}\psi = {} & \zeta\{J_0(\alpha)\sin(2\pi f_s\tau) + J_1(\alpha)[\sin(2\pi(f_s + f_d)\tau) - \sin(2\pi(f_s - f_d)\tau)] \\ & - J_2(\alpha)[\sin(2\pi(f_s + 2f_d)\tau) + \sin(2\pi(f_s - 2f_d)\tau)] + \cdots\} \\ & + \Gamma\zeta J_0(\alpha)[\sin(2\pi(3f_s - 2f_d)\tau) + \sin(2\pi(f_s - 2f_d)\tau)] \\ & - \Gamma\zeta J_1(\alpha)[\sin(2\pi(3f_s - 3f_d)\tau) + \sin(2\pi(f_s - f_d)\tau)] \\ & + \Gamma\zeta J_1(\alpha)[\sin(2\pi(3f_s - f_d)\tau) + \sin(2\pi(f_s - 3f_d)\tau)] + \cdots\},\end{aligned} \tag{3.9}$$

where the products of sinusoids have been expanded for the first three terms. Collecting like terms results in the model being expressed as

$$\begin{aligned}\psi = {} & \zeta J_0(\alpha)\left\{\sin(2\pi f_s\tau) + \frac{J_1(\alpha)}{J_0(\alpha)}\sin(2\pi(f_s + f_d)\tau)\right. \\ & - (1 + \Gamma)\frac{J_1(\alpha)}{J_0(\alpha)}\sin(2\pi(f_s - f_d)\tau) + \Gamma\sin(2\pi(3f_s - 2f_d)\tau) \\ & \left. + \left(\Gamma - \frac{J_2(\alpha)}{J_0(\alpha)}\right)\sin(2\pi(f_s - 2f_d)\tau) + \Gamma\frac{J_2(\alpha)}{J_0(\alpha)}\sin(2\pi(3f_s - 3f_d)\tau) + \cdots\right\},\end{aligned} \tag{3.10}$$

where only the six terms with the largest coefficients for the range of A^* tested have been retained. These six terms are the same as those presented in table 2. The coefficients of these six terms are also presented in the table, as well as the coefficients normalized by the coefficient of the first term.

It can be concluded that the model for the lift force as presented in (3.10) adequately accounts for all the frequencies of interest measured in the lift force data.

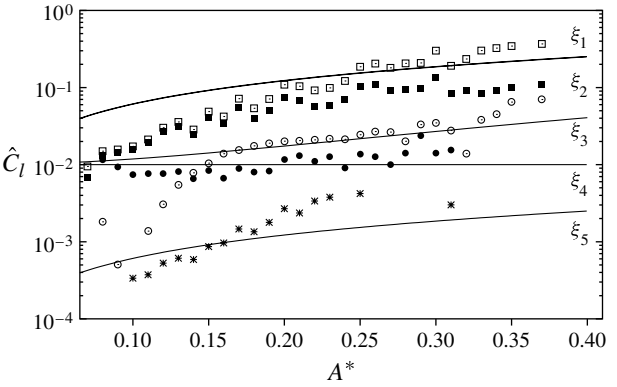

FIGURE 7. Strength of second to sixth strongest frequencies, normalized by the strength of the strongest frequency (points), compared to the second to sixth largest coefficients (ξ_1–ξ_5), normalized by the largest coefficient of (3.10) (lines). The definitions of ξ_1–ξ_5 are presented in table 2 (note that ξ_1 and ξ_2 are very similar, and are essentially overlaid on the plot). It is shown that the energy extracted from the data and the theoretical coefficients are of the same scale.

To recap, this model consists of the body generating waves at the new vortex shedding frequency f_s, which are then frequency modulated by the driving frequency f_d, which is then amplitude modulated by vortex interaction downstream.

The model of equation (3.10) can be further quantitatively tested by comparing the magnitudes of the coefficients to the energy content of each of the frequency components measured from the data. The absolute magnitudes of these terms cannot be gained without knowledge of the amplitude term ζ; however, if Γ is known, the ratio of the energy content of a given frequency to the energy content of the primary component at f_s can be calculated. As shown in (3.10) and table 2, Γ appears alone as the coefficient of the fourth term once the ratio with the primary term is taken. Therefore, Γ can be scaled by fitting to the data, allowing all of the other terms to be calculated.

Figure 7 compares the magnitude of the coefficients of each term in (3.10) to the energy of the six largest frequencies extracted from the data, over the range $0.05 \leqslant A^* \leqslant 0.40$. For the model, the coefficients have been normalized by the coefficient of the first term in (3.10), as presented in the fourth column of table 2; similarly for the data, the energy of each component has been normalized by the energy of the leading component.

While the coefficients of the model do not track the energy content of the components from the frequency spectra of the lift exactly, they are ranked in the same order, vary in the correct direction (i.e. generally increase with increasing A^*) and appear to be of the correct magnitude. This level of agreement indicates that the model captures the essential physics of the problem.

3.5. *Confirmation of the model at different values of Re*

To confirm the generality of the model presented in §§ 3.3 and 3.4, a simulation was conducted at $Re = 100$, to obtain a force time history for 1000 time units (approximately 160 shedding cycles). The amplitude of oscillation was set to $A^* = 0.20$. The driving frequency f_d was adjusted to again match the frequency of

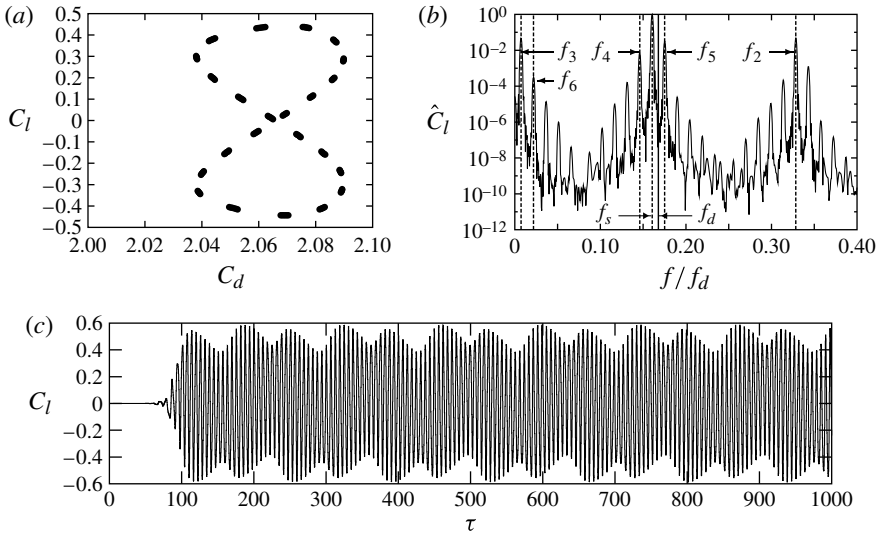

FIGURE 8. Results from a simulation at $Re = 100$, $A^* = 0.20$. (*a*) Poincaré sections of the lift coefficient against the drag coefficient, indicating that the flow is quasiperiodic. (*b*) Frequency spectrum of the lift force. The solid vertical line marks the Strouhal frequency for the unperturbed cylinder at $Re = 100$; the dashed vertical lines mark the frequencies outlined in table 2. The match between these frequencies and the prominent spikes of the spectrum shows that the results can be generalized to other values of Re. (*c*) The time history of the lift force, showing the modulated nature of the flow.

shedding from a fixed cylinder. A simulation of a fixed cylinder at $Re = 100$ was first conducted to deduce this frequency, which was found to be $f_d = 0.1679$.

The results of this simulation are shown in figure 8. Figure 8(*a*) shows the Poincaré sections of the lift coefficient against the drag coefficient. It appears that, as $\tau \to \infty$, the series of points on this plot will trace out a closed curve, indicating that the flow is quasiperiodic.

Figure 8(*b*) shows the frequency spectrum of the lift force on the body. A solid vertical line marks the driving frequency, and dashed vertical lines mark the frequencies defined in table 2. As for the flows at $Re = 175$, this series of frequencies represents the five leading frequencies presented in the lift force signal. Careful inspection shows that the sixth strongest frequency in the spectrum of figure 8 is not $3f_s - 3f_d$, as predicted by the model; however, $3f_s - 3f_d$ is the seventh strongest, and is of the same order as the sixth strongest frequency (which is four orders of magnitude smaller than the leading component). This level of agreement suggests that the amplitude- and frequency-modulated model proposed, based on data at $Re = 175$, is certainly valid at other values of Re, where the flow is two-dimensional.

Figure 8 shows the time history of the lift coefficient. This figure clearly shows the modulated nature of the flow, and confirms the conclusion drawn from the Poincaré section of figure 8(*a*) that the flow is quasiperiodic.

3.6. *Synchronization to P_N periodic states due to resonance between the vortex shedding and the driving*

The periodic states interleaved with quasiperiodicity, identified in figure 2, arise due to a synchronization between a subharmonic of the oscillatory driving and the new

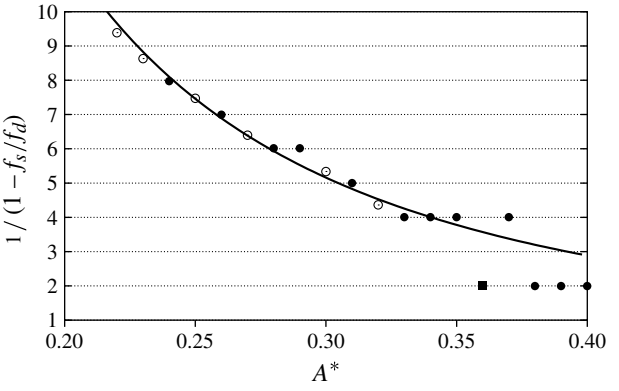

FIGURE 9. The ratio of the driving frequency to the difference between the driving frequency f_d and the new shedding frequency f_s, normalized by the driving frequency, $1/(1-f_s/f_d)$, as a function of A^*. The solid line shows this ratio using the dispersion relation of (3.1) for f_s; the points show this ratio using the peak frequency measured from the data. Plateaus in the relationship between this ratio and A^* in the measured data occur when the flow settles to a P_N periodic state, indicating synchronization between the new global vortex shedding frequency and the driving. When the flow settles to a P_N periodic state, this ratio is equal to N.

global vortex shedding frequency. There is more to this than just a simple fortuitous commensuration of the vortex shedding frequency f_s and the driving frequency f_d. The primary response frequency, f_s, is shifted from its 'natural' value stemming from the dispersion relation (see § 3.2.2), for a range of A^* around the value where this commensuration would occur. This results in small plateaus being formed in the relationship between f_s and A^*. This is illustrated in figure 9, which shows the ratio of the driving frequency to the difference between the driving frequency and the vortex shedding frequency. This ratio is then normalized by the driving frequency, to arrive at $1/(1-f_s/f_d)$.

The figure shows that, when this normalized ratio is an integer value N, the flow is synchronized to a P_N periodic state. The solid line in figure 9 comes from substituting the relationship for f_s defined in (3.1) into the ratio. The points come from extracting f_s from the data. The figure shows that the points 'step off' the curve, so that the ratio $1/(1-f_s/f_d)$ remains an integer value, at values of A^* where the flow is P_N periodic (this can be verified by referring to figure 2*b*).

In this paper, P_N periodic states for $N \leqslant 8$ have been identified. The data presented in figure 9 suggest that an essentially infinite series of states exist, with higher values of N as A^* is decreased. It appears that these states will have ever smaller bands of A^* over which they exist with increasing N, and therefore will be difficult to identify; their clear description remains an outstanding question.

4. Conclusions

For a cylinder performing inline oscillations at the frequency of vortex shedding from a stationary cylinder, a new vortex shedding frequency, f_s, is generated. This new vortex shedding process can be interpreted as the result of a wave generator. The generated waves at f_s are phase modulated by the oscillatory driving at the driving frequency f_d. Consideration of this phase-modulated signal can account for the first three frequencies present in the measured lift force data. The first six frequencies

can be accounted for by considering this phase-modulated signal also to be amplitude modulated. It is proposed that this amplitude modulation is due to the modification of the strength and position of the vortices shed from the body. This frequency- and amplitude-modulated model not only generates the correct frequencies, but also provides a measure of their relative strengths that compares well with the measured data. This model appears to account for the wake dynamics until the subharmonic mode loses stability at $A^* \simeq 0.65$. The success of this simplified model suggests that it is applicable at other values of Re, as long as the flow remains two-dimensional.

When the new vortex shedding frequency makes an integer ratio with the driving frequency, the flow selects a P_N periodic state, where $N = 1/(1 - f_s/f_d)$. For amplitudes close to those where the dispersion relation predicts f_s will make this integer ratio, the flow can synchronize to a P_N periodic state. States for $N \leqslant 8$ have been positively identified. The wake structure in these P_N periodic states can be highly complex, with large groups of vortices interacting over each repeating cycle.

The authors would like to acknowledge the help of Mr Y. L. Liew in the running of the simulations for this study, and the assistance of Mr P. Chan at the Monash Sun Grid computing facility. This work was financially supported under grant no. DP110102141 as part of the Discovery Grants program of the Australian Research Council.

REFERENCES

AL-MDALLAL, Q. M., LAWRENCE, K. P. & KOCABIYIK, S. 2007 Forced streamwise oscillations of a circular cylinder: locked-on modes and resulting fluid forces. *J. Fluids Struct.* **23**, 681–701.

BARBI, C., FAVIER, D. P., MARESCA, C. A. & TELIONIS, D. P. 1986 Vortex shedding and lock-on of a circular cylinder in oscillatory flow. *J. Fluid Mech.* **170**, 527–544.

BISHOP, R. E. D. & HASSAN, A. Y. 1964 The lift and drag forces on a circular cylinder oscillating in a flowing fluid. *Proc. R. Soc. Lond.* A **277** (1368), 51–75.

CARBERRY, J., SHERIDAN, J. & ROCKWELL, D. 2005 Controlled oscillations of a cylinder: forces and wake modes. *J. Fluid Mech.* **538**, 31–69.

CETINER, O. & ROCKWELL, D. 2001 Streamwise oscillations of a cylinder in a steady current. Part 1. Locked-on states of vortex formation and loading. *J. Fluid Mech.* **427**, 1–28.

CHOWNING, J. M. 1973 The synthesis of complex audio spectra by means of frequency modulation. *J. Audio Engng Soc.* **21** (7), 526–534.

FENG, L. H. & WANG, J. J. 2010 Circular cylinder vortex-synchronization control with a synthetic jet positioned at the rear stagnation point. *J. Fluid Mech.* **662**, 232–259.

GRIFFIN, O. M. & HALL, M. S. 1991 Vortex shedding lock-on and flow-control in bluff body wakes – review. *J. Fluids Eng.* **113** (4), 526–537.

GRIFFIN, O. M. & RAMBERG, S. E. 1976 Vortex shedding from a cylinder vibrating in line with an incident uniform flow. *J. Fluid Mech.* **75** (2), 257–271.

HOROWITZ, M. & WILLIAMSON, C. H. K. 2010 Vortex-induced vibration of a rising and falling cylinder. *J. Fluid Mech.* **662**, 352–383.

JAUVTIS, N. & WILLIAMSON, C. H. K. 2005 The effect of two degrees of freedom on vortex-induced vibration at low mass and damping. *J. Fluid Mech.* **509**, 23–62.

KARNIADAKIS, G. E., ISRAELI, M. & ORSZAG, S. A. 1991 High-order splitting methods of the incompressible Navier–Stokes equations. *J. Comput. Phys.* **97**, 414–443.

KARNIADAKIS, G. E. & TRIANTAFYLLOU, G. S. 1989 Frequency selection and asymptotic states in laminar wakes. *J. Fluid Mech.* **199**, 441–469.

KIM, B. H. & WILLIAMS, D. R. 2006 Nonlinear coupling of fluctuating drag and lift on cylinders undergoing forced oscillations. *J. Fluid Mech.* **559**, 335–353.

KONSTANTINIDIS, E. & BALABANI, S. 2007 Symmetric vortex shedding in the near wake of a circular cylinder due to streamwise perturbations. *J. Fluids Struct.* **23**, 1047–1063.

KONSTANTINIDIS, E., BALABANI, S. & YIANNESKIS, M. 2005 The timing of vortex shedding in a cylinder wake imposed by periodic inflow perturbations. *J. Fluid Mech.* **543**, 45–55.

KONSTANTINIDIS, E. & BOURIS, D. 2009 Effect of nonharmonic forcing on bluff-body vortex dynamics. *Phys. Rev.* E **79**, 045303(R).

KOOPMAN, G. H. 1967 The vortex wakes of vibrating cylinders at low Reynolds numbers. *J. Fluid Mech.* **28**, 501–512.

LEONTINI, J. S., STEWART, B. E., THOMPSON, M. C. & HOURIGAN, K. 2006 Wake state and energy transitions of an oscillating cylinder at low reynolds number. *Phys. Fluids* **18** (6), 067101.

LEONTINI, J. S., THOMPSON, M. C. & HOURIGAN, K. 2007 Three-dimensional transition in the wake of a transversely oscillating cylinder. *J. Fluid Mech.* **577**, 79–104.

LO JACONO, D., LEONTINI, J. S., THOMPSON, M. C. & SHERIDAN, J. 2010 Modification of three-dimensional transition in the wake of a rotationally oscillating cylinder. *J. Fluid Mech.* **643**, 349–362.

MORSE, T. L. & WILLIAMSON, C. H. K. 2009 Prediction of vortex-induced vibration response by employing controlled motion. *J. Fluid Mech.* **634**, 5–39.

NAZARINIA, M., LO JACONO, D., THOMPSON, M. C. & SHERIDAN, J. 2009 Flow behind a cylinder forced by a combination of oscillatory translational and rotational motions. *Phys. Fluids* **21** (5), 051701.

ONGOREN, A. & ROCKWELL, D. 1988 Flow structure from an oscillating cylinder. Part 2. Mode competition in the near wake. *J. Fluid Mech.* **191**, 225–245.

PERDIKARIS, P. G., KAITSIS, L. & TRIANTAFYLLOU, G. S. 2009 Chaos in a cylinder wake due to forcing at the Strouhal frequency. *Phys. Fluids* **21**, 101705.

SARPKAYA, T. 2004 A critical review of the intrinsic nature of vortex-induced vibrations. *J. Fluids Struct.* **19** (4), 389–447.

STAUBLI, T. 1983 Calculation of the vibration of an elastically mounted cylinder using experimental data from forced oscillation. *J. Fluids Engng* **105**, 225–229.

TANIDA, Y., OKAJIMA, A. & WATANABE, Y. 1973 Stability of a circular cylinder oscillating in uniform flow or in a wake. *J. Fluid Mech.* **61** (4), 769–784.

THIRIA, B., GOUJON-DURAND, S. & WESFREID, J. E. 2006 The wake of a cylinder performing rotary oscillations. *J. Fluid Mech.* **560**, 123–147.

THIRIA, B. & WESFREID, J. E. 2007 Stability properties of forced wakes. *J. Fluid Mech.* **579**, 137–161.

THOMPSON, M. C., HOURIGAN, K. & SHERIDAN, J. 1996 Three-dimensional instabilities in the wake of a circular cylinder. *Exp. Therm. Fluid Sci.* **12**, 190–196.

WILLIAMSON, C. H. K. & GOVARDHAN, R. 2004 Vortex-induced vibrations. *Annu. Rev. Fluid Mech.* **36**, 413–455.

WILLIAMSON, C. H. K. 1988 The existence of two stages in the transition to three-dimensionality of a cylinder wake. *Phys. Fluids* **31** (11), 3165–3168.